Gregson, F., Ordoubadi, M., Miles, R., Haddrell, A., Barona, D., Lewis, D., Church, T., Vehring, R., & Reid, J. (2019). Studies of Competing Evaporation Rates of Multiple Volatile Components from a Single Binary-Component Aerosol Droplet. *Physical Chemistry Chemical Physics*, *21*, 9709-9719 . https://doi.org/10.1039/C9CP01158G

ARTICLE

Studies of Competing Evaporation Rates of Multiple Volatile Components from a Single Binary-Component Aerosol Droplet

Received 00th January 20xx,
Accepted 00th January 20xx

DOI: 10.1039/x0xx00000x

F. K. A. Gregson[a], M. Ordoubadi[b], R. E. H. Miles[a], A. E. Haddrell[a], D. Barona[b], D. Lewis[c], T. Church[c], R. Vehring[b] and J. P. Reid[a,*]

The simultaneous evaporation and condensation of multiple volatile components from multicomponent aerosol droplets leads to changes in droplet size, composition and temperature. Measurements and models that capture and predict these dynamic aerosol processes are key to understanding aerosol microphysics in a broad range of contexts. We report measurements of the evaporation kinetics of droplets (initially ~25 µm radius) formed from mixtures of ethanol and water levitated within a electrodynamic balance over timescales spanning 500 ms to 6 s. Measurements of evaporation into a gas phase of varied relative humidity and temperature are shown to compare well with predictions from a numerical model. We show that water condensation from the gas phase can occur concurrently with ethanol evaporation from aqueous-ethanol droplets. Indeed, water can condense so rapidly during the evaporation of a pure ethanol droplet in a humid environment, driven by the evaporative cooling the droplet experiences, that the droplet becomes pure water within 0.4 s.

Introduction

The evaporation of droplets containing multiple volatile liquids under varying gas phase conditions is important for a range of industries. The drying of droplets containing multiple volatile and involatile components is an essential step in industrial manufacturing techniques such as spray-drying and delivery processes such as crop spraying and painting, and the evaporation of multicomponent fuels is an active area of research. [1] In drug delivery, inhalable active pharmaceutical ingredients (APIs) are often delivered as aerosols from pressurised metered dose inhalers in mixtures of propellants and co-solvents. Aerosolization is followed by rapid evaporation of the volatile components leaving the API and any involatile additives. [2] Quantifying the size of a resulting particle under different conditions is often imperative to the application; for example, the deposition fraction of particles in different areas of the lung is, among other factors, dependent on particle size and composition (including water content). [3] In addition, the dissolution rate, stability and rheology of spray-dried microparticles is very sensitive to the particle size and the drying history. [4–6] An improved understanding of droplet drying kinetics could lead to greater product control.

While the evaporation of micron-sized droplets features in countless applications, a quantitative understanding of the time-evolving size and composition of multicomponent droplets remains a challenge to measurements and models. Previous work has addressed the problem of multiple volatiles with different vapour pressures, considering the need to represent internal concentration profiles within a Maxwell-Stefan framework.[7,8] We now move towards systems of competing evaporation rates with components of similar volatility. In such systems, an array of different transport mechanisms compete on similar timescales. Mass transfer between the condensed phase and gas phase is coupled to heat transfer, a consequence of the latent heat expelled during the conversion of liquid to vapour. When more than one component is present, diffusional mixing can act to maintain a homogeneous composition throughout a particle during evaporation. Alternatively, if the rate of evaporation is large, the droplet may become radially inhomogeneous if the mixing rate cannot compete with the rate of surface recession. [9]

Studying the kinetics of evaporation of micron-sized droplets is challenging because of the speed of the drying process and because of the technical challenges associated with performing *in situ*

[a] School of Chemistry, University of Bristol, Bristol, BS8 1TS, UK
[b] Department of Mechanical Engineering, University of Alberta, Edmonton, AB, Canada
[c] Chippenham Research Centre, Chiesi Limited, Chippenham, Wiltshire, SN14 0AB, UK

Electronic Supplementary Information (ESI) available: [details of any supplementary information available should be included here]. See DOI: 10.1039/x0xx00000x

measurements. However, single particle techniques can provide insight into the drying processes. [10] Reports of measurements of the kinetics of evaporation or condensation of single aerosol droplets have been provided in numerous publications, [11–13] wherein a droplet is isolated through an electrodynamic trap or optical levitation or tweezing. The rates of mass transfer in such experiments are often slow such that the process can be assumed to be isothermal and steady. Semi-analytical approaches to predict the kinetics of condensation or evaporation of unary or binary droplets can be derived. However, these approaches rely on the assumption that quasi-steady-state mass and heat fluxes are uncoupled. [14]

In the previously mentioned applications of pulmonary drug delivery, fuel-delivery for combustion and spray-drying, evaporation is typically unsteady and the differential equations for mass and heat transfer must be solved simultaneously as they are strongly coupled. Previous studies have observed the evaporation kinetics of rapid droplet drying, with time scales on the order of milliseconds, using a free-falling droplet chain in a gas-flow of dry-nitrogen. [15,16] The evolution of composition during the evaporation of ethanol-water droplets has been studied using cavity-enhanced Raman scattering (CERS) on a falling droplet train. [17] The preferential evaporation of ethanol was observed initially, owing to its higher volatility than water. In many applications, the gas phase surrounding droplets is humid and, thus, not only evaporation but gas-particle partitioning from the vapour phase onto the droplet (i.e. condensation) must be considered. Whilst there are existing models that have been shown to treat the droplet temperature explicitly in evaporating droplets,[17,18] here we validate a modified Maxwell equation with sophisticated experimental data that highlight the implications of this temperature drop: competing evaporating rates and condensation from the vapour phase onto the droplet.

In this work, we report studies of the evaporation of droplets formed from mixtures of ethanol and water of ~25 µm radius levitated within a comparative-kinetics electrodynamic balance (CK-EDB) over timescales spanning 500 ms to 6 s. The CK-EDB instrument allows control over both the relative humidity (RH) and temperature within the gas phase. Ethanol and water are chosen as a benchmark system for study because of the accuracy with which their transport properties in the gas and condensed phases are known, the similarity in their refractive indices, the precedent in the literature for studying the evaporation of single component water and ethanol droplets, and their relevance for processes such as drug delivery to the lungs. We introduce the experimental methods in Section 2 before presenting measurements of the evaporation kinetics of pure ethanol and mixed ethanol-water droplets in dry and humid air, Section 3. The measurements are compared with a numerical model that captures the heat and mass transfer during the evaporation and condensation processes, and we consider the uncertainties in the model predictions and measurements that must be understood when comparing them. We conclude by examining the competing evaporation and condensation of ethanol and water, respectively, when pure ethanol droplets evaporate in a humid atmosphere.

Experimental

The evaporation of single aerosol droplets containing mixtures of water and ethanol was studied using a CK-EDB. In all experiments, HPLC grade water (Fisher Scientific) and absolute grade ≥ 99.8% ethanol (Sigma Aldrich) was used. This approach has been described in detail in a previous publication [19] so will only be briefly discussed here. A single, charged droplet (~ 25 µm radius) of known initial composition is produced by a droplet-on-demand generator and injected into the centre of an environmentally controlled chamber, where it is trapped by the presence of an electrodynamic field. The droplet is confined within the centre of two sets of concentric cylindrical electrodes mounted vertically opposite one another. The electrodynamic field is produced by applying an AC voltage across the inner pair of electrodes. An additional DC voltage is applied to the lower electrode to counteract the gravitational force acting upon the droplet. The temperature of the trapping chamber (variable from 273 K to 323 K) is controlled by circulating ethylene glycol coolant around the electrodes. A gas flow of controlled RH (<10 to <90%) formed from mixing wet and dry nitrogen flows passes over the trapped droplet with a speed of typically 0.03 m s^{-1}.

The droplet is illuminated with a 532 nm continuous-wave laser, with interference between the reflected and refracted rays leading to a characteristic angularly-resolved elastic-scattering pattern consisting of light and dark fringes (phase-function). The phase-function is collected by a CCD centred at 45° to the forward scattering direction, over an angular range of ~24°. The angular separation between the

fringes in the phase-function, $\Delta\theta$, can be used to estimate the droplet radius, *r*, using the geometrical optics approximation to Mie theory:

$$r = \frac{\lambda}{\Delta\theta}\left(\cos\left(\frac{\theta}{2}\right) + \frac{n\sin\left(\frac{\theta}{2}\right)}{\sqrt{1+n^2-2\,n\,cos\left(\frac{\theta}{2}\right)}}\right)^{-1} \quad (1)$$

where λ is the laser wavelength, ϑ is the central viewing angle and n is the droplet refractive index. This approximation has been shown previously to determine the radius to an accuracy of ± 100 nm. [20]

A comparative kinetics approach is used to determine the exact RH at the trapping position by measuring the evaporation kinetics of a probe droplet prior to the sample ethanol-water droplet of interest. For RHs above 80%, a probe water droplet is used. The evaporation kinetics are fitted using the semi-analytical model of Kulmala et al. to determine the RH to an accuracy of ~ ± 1%. [14] For RHs between 45% and 80%, an aqueous NaCl probe droplet is used by probing the final equilibrated size of the droplet: the RH is determined from the growth factor corresponding to the equilibrated particle radius and a parameterisation based on the E-AIM model, to an accuracy of ~ ± 1%. [21] This comparative kinetics approach for determining gas phase RH has previously been validated for a range of inorganic compounds.[20] For RHs below 45%, an approximate RH is determined by using the ratio of dry to wet nitrogen flows set on the mass-flow controllers, with an accuracy of ~ ± 2%.

All data are collected assuming that the droplet refractive index remains constant throughout the evaporation process at 1.3360, equivalent to that of pure water at λ =532 nm. No further correction is made to account for the ethanol present in the droplet due to the similarity in its refractive index (1.3614 at λ = 532 nm) to that of water. [22] There is a dependence of the refractive index of water on the droplet temperature, which in this study varies over ~ 20 K. However, the refractive index of water between 273 K and 293 K varies by only 0.001 and, hence, this effect can be neglected in this work. [23]

Results and Discussion

We first discuss measurements of the evaporation kinetics of both pure ethanol droplets and mixed ethanol-water droplets evaporating into a dry nitrogen atmosphere in the CK-EDB. The evaporation kinetics at a range of gas phase temperatures are compared. We then explore the evaporation kinetics of mixed ethanol-water droplets into varying relative humidities. We introduce a numerical model for simulating the evaporation of ethanol-water droplets, providing time-dependent predictions of the evolving droplet radius, droplet temperature and the changing concentration of the two volatile components present in the droplet. We then use the model to explore the interesting case of a pure ethanol droplet evaporating into high RH conditions.

Evaporation of Pure Ethanol and Mixed Ethanol-Water Droplets in Dry Nitrogen

We begin by considering the general trends observed in the evaporation kinetics of droplets containing only volatile components. A measurement of the time-dependent radius-squared of a pure ethanol droplet evaporating in the CK-EDB into dry nitrogen at a gas phase temperature of 293 K is shown in Fig. 1 (red triangles). The evaporation proceeds in a constant rate until ~ 0.4 s when the evaporation rate decreases. This reflects the effective distillation of the two components: it is expected that ethanol, with a higher volatility, evaporates faster leaving water remaining in the droplet.

The mass flux, I_m, during the isothermal evaporation of single component droplets at the same temperature as the gas phase can be calculated from the Maxwell equation: [24]

$$I_{\mathrm{m}} = 4\,\pi\,D\,r\,(C_{\mathrm{s}} - C_{\infty}) \quad (2)$$

where *D* is the mass diffusivity of the vapour component in the gas phase, [25,26] *r* is the droplet radius and *C* is the vapour concentration one mean-free path from the droplet surface (subscript s) or far from the droplet (subscript ∞). This equation is derived assuming that the evaporation is gas-diffusion controlled, in the continuum regime, with negligible effects from Stefan flow and the Kelvin effect. Expression in terms of the rate of radius-change (rather than mass change) and integration leads to the radius-squared rule:

$$r^2 = {r_0}^2 - \left(\frac{2\,D\,M_i\,p_i^0(T)}{\rho_i\,R\,T}\right)(t - t_0) \quad (3)$$

where ρ_i is the density of the droplet, M_i is the molar mass of the evaporating component, p_i^0 is the vapour pressure of the evaporating component at droplet temperature *T* and *R* is the molar gas constant. Evaluation of Equation 3 leads to a constant gradient in

radius-squared with time, *t*. Thus, for comparison with the measurements, we have included in Fig. 1 the expected gradients for pure ethanol droplets with the same starting radius as the experimental data evaporating at a range of gas phase temperatures. In these simulations, the vapour concentration at the droplet surface was calculated using the temperature-dependent vapour pressure of ethanol and assuming that the droplet was at the same temperature as the gas phase. The gas phase is assumed to be devoid of ethanol. As might be anticipated, the measured evaporation rate of pure ethanol into dry nitrogen at 293 K is not well represented by the radius-squared rule when the droplet temperature is assumed to be the same as the gas phase temperature. Indeed, to accurately reflect the gradient recorded in the experimental data, the assumed droplet temperature must be reduced to 276 K, which is the wet-bulb temperature in this case. This demonstrates the extent to which the mass and heat flux during this rapid evaporation process are coupled, and the need for a numerical model that can consider the effect of temperature suppression on the kinetics of such a rapidly evaporating droplet. [27]

Qualitatively, as the ethanol droplet evaporates, the ethanol molecules transitioning from the liquid state (the droplet) to the vapour state (the gas phase) remove energy from the droplet in the form of the latent heat required for vaporisation. As expected, this loss of energy is manifested as a decrease in the surface temperature of the droplet, which undergoes rapid cooling as the evaporation progresses. The cooling at the droplet surface reduces the vapour pressure of ethanol, which in turn reduces the evaporation rate. Thus, the experimental measurement of a pure ethanol droplet evaporating into dry nitrogen in the CK-EDB at a gas phase temperature of 293 K is slower than estimated by a simple radius-squared rule at the same temperature.

The time-dependent radius-squared of a droplet containing a mixture of ethanol and water (70% and 30% by weight, respectively), evaporating into dry nitrogen at 293 K, is also shown in Fig. 1 (blue squares). The pure component vapour pressure of ethanol at 293 K is greater than that of water (5.7 KPa for ethanol [28] compared to 2.34 kPa for water at 293 K [29]), so it is expected that the ethanol will evaporate more rapidly from the droplet at early time, followed by evaporation of the water. Indeed, the non-uniform evaporation profile with two linear sections separated by an inflexion point at approximately 0.5 s is consistent with this expectation, reflecting the effective distillation of the two components with differing volatilities. The initial evaporation rate of the mixed droplet is lower than that of the pure ethanol droplet due to the presence of water reducing its vapour pressure. The Henry's law activity coefficient for ethanol in 70% wt/wt aqueous ethanol system is 0.59, meaning that the vapour pressure of ethanol in the initial droplet is 3.5 kPa compared to the 5.7 kPa if it were pure ethanol at 293 K. [30,31] For water, the activity coefficient in this initial composition of 70% ethanol : 30% water is 0.71, reducing the vapour pressure to 1.7 kPa from a value of 2.3 kPa for pure water. However, the final evaporation rate of the mixed droplet is very close to that of the simulated evaporation profile of a pure water droplet under the same conditions, also shown in Fig. 1. The black line in Fig. 1 shows a simulation of a pure water droplet evaporating in dry nitrogen at 293 K, using the K-V-H model presented by Su et al. [32] This simulation, which accounts for evaporative cooling caused by coupled heat and mass transfer in the evaporation of pure water, shows a gradient which very closely matches the final gradient in the 70% ethanol : 30% water droplet, within the uncertainty of RH (± 2%) and temperature (± 1.5 K). This demonstrates that in the later stages of this measurement, the ethanol has completely evaporated, leaving a pure water droplet. Indeed, the water simulation starts with a volume equivalent to the quantity of water present in the mixed ethanol-water droplet. The transition in gradient rather than an abrupt change indicates that there is not a defined period of ethanol evaporation followed by water evaporation; rather, the co-evaporation of both components occurs, with a gradual decrease in ethanol composition until only a pure water droplet remains. The grey circles in Fig. 1 show a droplet containing 50% ethanol : 50% water evaporating into dry nitrogen. It can be seen that with a decrease in initial ethanol content the time that the evaporation rate decreases occurs earlier. The second linear stage of evaporation shows an approximately equal evaporation rate to that of the 70%:30% mixed droplet, supporting the theory that the droplet is pure water at this time.

The evaporation of mixed component droplets (70% ethanol : 30% water by weight) was repeated at a range of gas phase temperatures from 273 K to 293 K (see Fig. 2). As the gas phase temperature is reduced, the vapour pressures of both ethanol and water are lowered and, thus, it takes longer for the droplet to evaporate. The transition from a majority-ethanol droplet to one which is mostly

water, appears to shift to later times and becomes a smoother transition with reduction in temperature. This can be attributed to the temperature-dependent vapour pressure of ethanol and water being closer at colder temperatures, as shown in the Supplementary Information. Although in Fig. 2 the evaporation appears to proceed with an equivalent rate at 293 K and at 285 K, the initial droplet size for the data at 293 K is larger, hence the evaporation rate is greater. This can be seen more clearly in the Supplementary Information where a version of this plot is presented which is normalised with respect to the initial r^2.

The measurements in Fig. 1 and 2 demonstrate that, even for the simplest cases of pure ethanol or mixed ethanol-water droplets evaporating into a dry nitrogen atmosphere, the kinetics of the evaporation process are complicated by the effect of evaporative cooling. This supresses the component vapour pressures at the droplet surface. In addition, the concurrent evaporation of ethanol and water leads to temporal variations in size that show complex, non-monotonic behaviour. In the next section we will discuss the more complex situation of ethanol and ethanol-water droplet evaporation into a humid atmosphere.

Evaporation of Mixed Ethanol-Water Droplets in Humid Nitrogen

The time-dependent radii of droplets containing 50% ethanol : 50% water (wt/wt) as they evaporate at 293 K into environments of different RH in the CK-EDB are presented in Fig. 3. The droplet evaporation profiles in humidified nitrogen show much more pronounced transitions in evaporation rate than in the experiments carried out in dry nitrogen in Fig. 1 (grey circles). The evaporation event appears to proceed in two stages. First, the initial rapid evaporation of ethanol occurs with a rate that appears to be largely independent of the RH. This is followed by a second stage characterised by the slow evaporation of water. As expected, this second stage shows a strong dependence on the RH in the gas phase, consistent with the assumption that it is largely determined by water evaporation.

In the CK-EDB, trapped droplets undergo evaporation within a gas flow which passes over the droplet surface, continually refreshing the droplet environment. For droplets evaporating into dry conditions, the presence of the gas flow means that it can be assumed that the volume of gas surrounding the droplet is infinite and continuously replenishes dry nitrogen to the droplet surface. Hence, for droplets evaporating into dry conditions, re-condensation of the evaporating component from the gas phase back onto the droplet cannot occur. However, when water is present in the gas phase, i.e. a non-zero RH, the droplet evaporation process is complicated by the possibility of gas-to-particle partitioning. Condensation of water from a humid environment onto a droplet can occur if the vapour pressure at the droplet's surface is lower than the partial pressure of water vapour in the gas. At room temperature, ordinarily the condensation of water onto a water droplet evaporating under sub-saturated conditions (i.e. an RH < 100%) cannot occur. However, the rate of ethanol evaporation at 293 K is on the order of 1×10^{-10} kg s^{-1}, which is sufficient to cause evaporative cooling of the droplet of around 17 K, as demonstrated in Figure 1. The evaporative cooling decreases the saturation vapour pressure of water at the droplet surface, which may become low enough that it exceeds the partial pressure of water in the gas flow at the ambient temperature, leading to a supersaturation with respect to water vapour in the surface region which results in the condensation of water from the gas phase onto the droplet as the ethanol evaporates. [33] This is in agreeement with previous observations of water condensation onto much larger evaporating droplets, such as ethanol drops deposited on a surface [34] or acoustically-levitated droplets containing 1-butanol, [35] both on the order of millimetres in radius.

Comparison of Measurements of Multicomponent Evaporation of Ethanol–Water Droplets with a Numerical Model

A modified quasi-steady model based on the Maxwell equation appropriate for multicomponent systems is employed to study temperature, composition and size histories of the droplets in conjunction with the CK-EDB data. The model accounts for the non-ideal mixing of water and ethanol in both density and activity coefficients and calculates the temperature and mass of the droplet from the superposition of the effects of each individual component in the equations of conservation of mass and energy. It also accounts for simultaneous evaporation and condensation of different species. The interaction of different vapours with each other is ignored and it is assumed that the vapour diffusion of one vapour does not affect the diffusion of the other component. Also, it is assumed that the

liquids mix infinitely fast and the temperature is uniform across the droplet, although it can change with time.

The net evaporation rate of the droplet, I_m is obtained from Equation 2. In this equation C_s for each component i is obtained from the modified Raoult's law using the temperature, composition and activity coefficients of different liquid components in the mixture at each time-step. The droplet temperature, T_s, is obtained from:

$$\rho C_p \frac{r^2}{3}\frac{dT_s}{dt} = -\bar{k}(T_s - T_\infty) - \sum L_i D_i \left(C_{s,i} - C_{\infty,i}\right) \quad (4)$$

where ρ, C_p, $\bar{k}$, T_∞ and L_i are the droplet density, droplet specific heat capacity, the gas thermal conductivity at an intermediate temperature around the droplet [36] and the latent heat of vaporization of component i, respectively. The droplet density can be obtained from empirical relationships available for the mixtures of interest. For example, to account for the no-ideal mixing of water and ethanol, the relationship proposed by Khattab *et al.* is used in this study. [37] The other transport and material properties such as the vapor diffusion coefficients, latent heats of vaporization, specific heats and gas thermal conductivities were obtained from appropriate temperature dependent correlations. [38–41]

Fig. 4 shows the measured evaporation profiles from Fig. 3, compared to those predicted by the numerical model. The shading refers to the effect on the model predictions of the uncertainty in the experimental conditions, such as RH, temperature and initial droplet radius. The model successfully reproduces the two distinct evaporation stages corresponding to the rapid loss of ethanol and slower loss of water, with good agreement seen between the predicted time when the evaporation rate changes and that observed experimentally. Whilst the model lies very close to the experimental data in panels (a), (c) and (e), there is a discrepancy with the data in panels (b) and (d). Possible causes of this discrepancy will be discussed later in this section.

The initial large mass-flux of ethanol from the droplet induces a reduction in the droplet temperature, as demonstrated in Fig. 1. If the droplet cools sufficiently, the partial pressure of water vapour present in the gas phase due to the RH in the gas flow will lead to supersaturation at the cooled droplet surface, inducing water condensation from the gas phase onto the droplet. [33] This is not too dissimilar from the process that drives the condensation of water onto aerosol particles to form cloud droplets: a supersaturation of water in the gas phase in a rising and cooling air parcel drives water condensation. [42] Here, we see a combination of ethanol evaporation and water condensation during the first stage of the evaporation process.

The predicted changing droplet compositions throughout the evaporation process at different RHs are shown in Figure 5a. The figure shows the initial rapid loss of ethanol mass from the droplet over a period of around 0.2 – 0.3 s. The resultant cooling of the droplet leads to the condensation of water from the gas phase, increasing the mass of water in the particle. The larger the relative humidity, the greater the mass of water condensation on to the droplet as the degree of supersaturation at the surface will be higher. The time at which net water condensation on to the particle changes to net water evaporation coincides with the point at which all ethanol has been lost from the droplet. Figure 5b shows the predicted droplet temperature within the first 0.7 s of evaporation; an initial rapid cooling of the droplet due to ethanol evaporation is observed, followed by a much slower increase in temperature due to the latent heat deposited in the droplet by the condensing water molecules. When all ethanol has been lost, the droplet temperature is observed to remain suppressed, but steady. As expected from Equation 4, the degree of droplet temperature suppression is largest for the droplet with the fastest evaporation rate (lowest gas phase RH).

The time of the change in evaporation rate, seen in Figure 4, corresponds to the time at which there is an apparent reversal in the direction of the water mass-flux in Figure 5. The radius at which this occurs is directly related to the mass of water that condenses onto the droplet in the first ~ 0.3 seconds. This depends on the droplet initial starting composition (mass fraction of ethanol), the specific latent heats of vaporisation of water and ethanol, the initial droplet starting size and the gas phase RH. There are multiple possible sources of uncertainty both in the experiment and in the model, however the agreement between the model and experimental data is reasonable. We have considered all sources of experimental error and their effect on the model output in the following section. The model describes the evaporation and condensation process with an agreement to the experimental data that we believe it close enough for the model to make valuable predictions for other similar cases of

multiple volatile components, relevant to a variety of important applications.

Uncertainties in Evaporation Measurements and Sensitivities of Model Predictions

Uncertainties in the measurements and assumptions about their interpretation could lead to an incorrect choice of parameters used in the model comparison. The model agrees with the experimental data capturing the change in evaporation rate representing the reversal of water mass-flux, although the model does consistently underestimates the radius at this point. This suggests that the model underpredicts the extent to which water condenses onto the droplet during the period of ethanol evaporation. Factors in the experiment that affect the interpretation of the mass of water in the droplet at the end of the first stage of evaporation include uncertainties in the initial droplet composition, the initial droplet size and the gas phase RH. Whilst efforts were made to minimise the time between solution preparation and CK-EDB measurements, the volatilities of ethanol and water are sufficiently high that the starting droplet composition may not be exactly that intended. This has been discussed in more detail in the supporting information, where Fig. S3 presents model calculations for the data in Fig. 4a – 4d, with a variation in the initial assumed composition of the droplets. The extent to which the initial composition must be changed to get the model and data to fully match is greater than can be realistically expected, but may be a contributory factor in the experimental uncertainty.

The numerical model also relies on an accurate value of the initial droplet radius. As the droplet is produced outside the CK-EDB by the droplet-on-demand generator and injected into the trapping chamber, there is a flight-time of approximately 0.1 s before the droplet is trapped and no measurement of droplet size is possible prior to this time. In previous work with aqueous aerosol droplets, the initial droplet size was estimated by a linear back extrapolation of the temporal dependence of the radius-squared (r^2) recorded immediately following droplet capture. [43] However, the initial evaporation rate of an ethanol-water droplet is likely to be non-linear in r^2 with time, particularly at early time and in the early stages of evaporation. This is explored in more detail in the supporting information. We show that an extrapolation using a 2nd order polynomial fit of r^2 versus time in the initial part of the data gives a larger initial droplet radius, and an improvement of the agreement between the model and the data. An error in the initial starting radius of 1.45 µm would cause the model to fully match the data and, whilst this is not a plausible error, we show that this is still a possible contributing factor to the experimental uncertainty.

The final experimental factor which impacts the accuracy of the model prediction is the measurement of the gas phase RH. As described earlier in the manuscript, the gas phase RH in the trapping chamber is determined immediately prior to an ethanol-water droplet evaporation measurement using a probe droplet containing either pure water or aqueous sodium chloride. This method for determining the RH has been reported by us previously and has been demonstrated to have accuracies far in excess of those available with commercial relative humidity probes or with assuming a particular value based on the ratio of the gas phase mass flow rates of humid and dry air. [20,43,44] The effect of the uncertainty in the RH retrieved using the probe droplet on the ethanol-water evaporation profile is shown by the shaded regions in Figure 4. The magnitude of the uncertainty is insufficient to explain the disagreement between the model and the measurement.

The mass of water calculated to condense on to an evaporating ethanol-water droplet is highly dependent on the extent of the droplet surface temperature suppression. This is shown in Figure 5b for the four cases of 50% ethanol : 50% water droplet evaporations shown in Figure 4. All show a similar shape of the time-dependent droplet temperature profile, with an initial sharp drop in temperature as ethanol evaporates, followed by the droplet warming and equilibrating at a constant temperature when the evaporating species becomes solely water. This equilibrium temperature is reached when the energy lost from the droplet due to the evaporating mass flux of water is balanced with the thermal energy supplied to the droplet from the gas phase. The model calculates the droplet temperature using an energy-balance approach with the aggregate mass flux: it considers both the negative mass flux of ethanol and positive mass flux of water. If the model underpredicts the magnitude of the droplet temperature suppression, the mass of water calculated to condense on to the droplet will also be underestimated, leading to a lower predicted radius at the inflection point than would be seen experimentally. The implications of a droplet temperature suppression are explored further in the next section.

The Evaporation of Pure Ethanol Droplets in Dry and Humid Nitrogen

The measured evaporation profile of a pure ethanol droplet into nitrogen at 91% RH and 293 K is shown in Figure 6a and is compared to the profile of a pure ethanol droplet into dry nitrogen at 293 K. In dry nitrogen gas, the pure ethanol droplet is observed to evaporate at a constant rate throughout its lifetime. This is shown from the inset in Figure 6a. By contrast, the evaporation of a pure ethanol droplet in humid nitrogen proceeds through two distinct stages of mass flux, similar to those observed for the case of the mixed ethanol-water droplets shown in Figure 4. This difference in the droplet behaviours can be explained as follows.

In both instances, the ethanol droplets undergo rapid cooling due to the removal of energy from the droplet caused by the evaporation of the ethanol. As discussed previously, this decrease in temperature leads to a reduction in the saturation vapour pressure of water at the droplet surface. For the droplet evaporating into humid nitrogen, the saturation vapour pressure of water decreases below the partial pressure of water in the gas phase, leading to supersaturation of water vapour at the droplet surface, and causing condensation of water from the gas phase on to the droplet. This changes the droplet composition from a pure ethanol droplet to a pure water droplet, once the ethanol has evaporated, giving the two distinct evaporation stages. This changes the droplet composition from a pure ethanol droplet to a pure water droplet, giving the two distinct evaporation stages. Conceptually this is a very important result, as it shows that droplets which are initially non-aqueous undergoing rapid evaporation in a humid environment can become significantly water enriched through condensation of water vapour from the gas phase. For the ethanol droplet evaporating into dry nitrogen, there is no water vapour present in the gas phase and so the relative humidity in the flow remains zero. This is in agreement with a previous report of the importance of air humidity on the presence of condensed water or ice onto evaporating propellant droplets in spray-driers. [45]

The change in composition of the ethanol droplet evaporating into the humid environment is confirmed by the model simulations in Figure 6b, which shows predictions of the time-dependent droplet temperature and the time-dependent droplet composition. The large mass flux of ethanol at times earlier than 0.4 s causes the droplet surface temperature to initially cool to ~6 K lower than the gas phase temperature, inducing a supersaturation of 150% at the droplet surface set by the partial pressure of water in the surrounding gas phase at 293 K. This leads to a complete switch in the droplet composition as water vapour from the humid gas phase condenses on the cooled droplet surface; after 0.4 seconds the composition of the originally ethanol droplet becomes completely that of water. The magnitude of the initial temperature suppression predicted by the model under humid conditions is not as large as the ~ 15 K temperature suppression estimated for a pure ethanol droplet evaporating in dry air, predicted with a simple Maxwell simulation, as shown in Fig. 1. The condensation of water onto the droplet from the gas phase releases energy and mitigates, to some extent, the evaporative cooling from the loss of ethanol.

The amount of water that can condense onto an evaporating droplet is indeed affected by the magnitude of temperature suppression, but also by the initial droplet composition. To compare the data at 91% RH in Fig. 5 with the data also at 91% in Fig. 6, there is a much greater degree of water accommodation onto the droplet that was initially pure ethanol, than onto the droplet that was a 50% mix of ethanol and water (1.4×10^{-12} kg compared to 0.4×10^{-12} kg, respectively). In both cases, the gas phase RH was 91%. The rate of ethanol evaporation was similar, as there is no ethanol vapour in the gas-phase, so for both cases the droplet temperature was ~ 288 K. However, when the initial droplet composition is pure ethanol there is more ethanol to evaporate, so the timeframe at which the droplet is cooled lasts longer (0.5 s). Additionally, there is a value of zero water-activity in the droplet, so the rate of water condensation during this cooled period is faster. When there is a 50% mix of ethanol and water initially, the water activity is non-zero, hence the rate of condensation is reduced compared to the pure ethanol droplet, as well as a slightly shorter time at which the droplet is cooled (0.3 s). Hence, when the initial droplet is pure ethanol, there is a greater mass of water condensing on compared to the mixed droplet.

The large degree of water condensation occurring onto the droplet during ethanol evaporation has broader implications for understanding volatile droplet evaporation, particularly in the field of respiratory drug delivery. The formulations used in metered dose inhalers typically contain highly volatile propellants with large evaporation rates. The results from this work show that such a droplet would evaporate very quickly. The RH in the human lung has

been shown to reach around 99.5%, [46] so the effect of evaporative cooling acting on the droplet surface could cause a rapid switch in composition to only consist of the drug in water after just a few hundred milliseconds. The evaporation profile of how the drug behaves in water, as opposed to in the manufactured solvent and propellant, must then be accounted for when considering droplet size distributions, the disposition of APIs on deposition, and lung deposition fraction. [2]

Conclusions

This study demonstrates the extent to which mass and heat flux are coupled during the evaporation of micron-sized droplets of water and ethanol mixtures. A detailed understanding of droplets containing mixtures of volatile components behave in atmospheres of different temperatures and relative humidities is essential for a range of industries. A model has been developed that validates the experimental evidence of rapid condensation of water occurring concurrently with ethanol evaporation, which impact applications in spray drying and drug delivery. Formulations containing multiple volatile components are prevalent in a wide range of important applications and the model presented in this work will be of use to predict the evaporation kinetics under many different conditions. We demonstrate the importance of considering the droplet temperature in kinetic modelling: the rapid evaporation of droplets in humid atmospheres can lead to condensation from the gas phase onto the droplet surface. The evaporation rates of propellants typically used in metered dose inhalers can be much greater than ethanol; hence evaporative cooling of such a droplet can be expected to have an enormous effect on the evaporation kinetics, and lead to a large degree of water condensation. The subsequent evaporation of the condensed water can lead to a droplet having much longer lifetimes than expected, which is important to consider in spray-drying and inhalation models. We have presented results on ethanol and water as volatile components in a single droplet, however the results of this work are applicable to a range of different volatile solvents. In the field of spray-drying there would be additional involatile salts present. The variation in droplet temperature caused by multiple solvents evaporating at different rates, demonstrated here, could cause changes to parameters such as the droplet viscosity and surface tension, which would be expected to lead to significant differences in the morphology, density and degree of crystallinity for the final product. Whilst the model and experimental data presented here have inherent uncertainties, outlined in detail in the supporting information, this work represents a significant step-forward in the understanding and prediction of the kinetics of rapidly evaporating aerosol droplets containing multiple volatile components.

Conflicts of interest

There are no conflicts to declare

Acknowledgements

This work was supported by the EPSRC under grant code EP/N025245/1. RV acknowledges support for this work from the Natural Sciences and Engineering Research Council of Canada, Grant RGPIN-2016-04111. The experimental data presented in the figures are provided through the University of Bristol data repository at Reid, J. P. (2019): DOI: 10.5523/bris.16u0rx4tgbgx31zkqx6gn25whb.

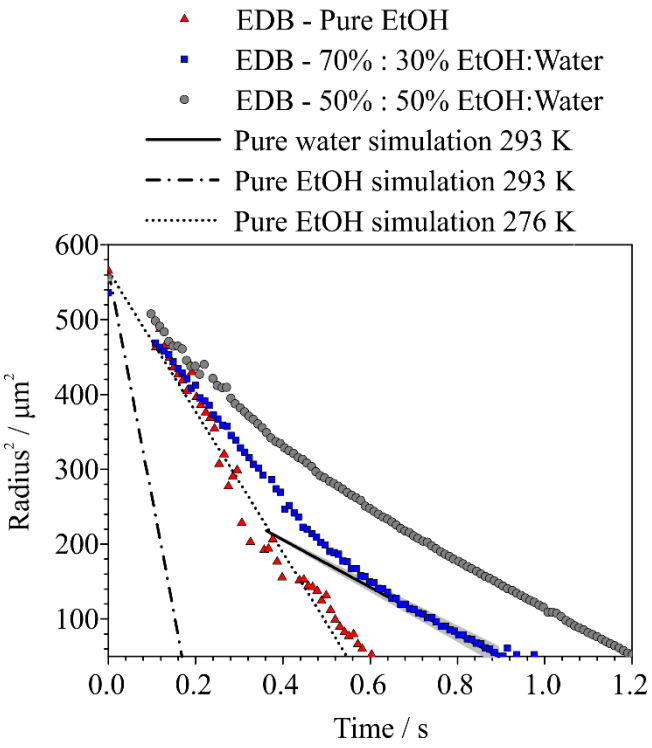

Figure 1: The evaporation of a droplet containing 70% ethanol : 30% water (wt/wt) into dry nitrogen at 293 K (blue squares) compared to that of a pure ethanol droplet under the same conditions (red triangles). Dashed lines show predicted ethanol evaporation profiles at 276 and 293 K simulated using Maxwell's equation. The black line shows a theoretical evaporation profile of a pure water droplet of equivalent volume to that present in the 70% ethanol :30% water mixture, at 293 K in dry nitrogen. Grey circles show the evaporation of a droplet containing 50% ethanol : 50% water (wt/wt) into dry nitrogen at 293 K.

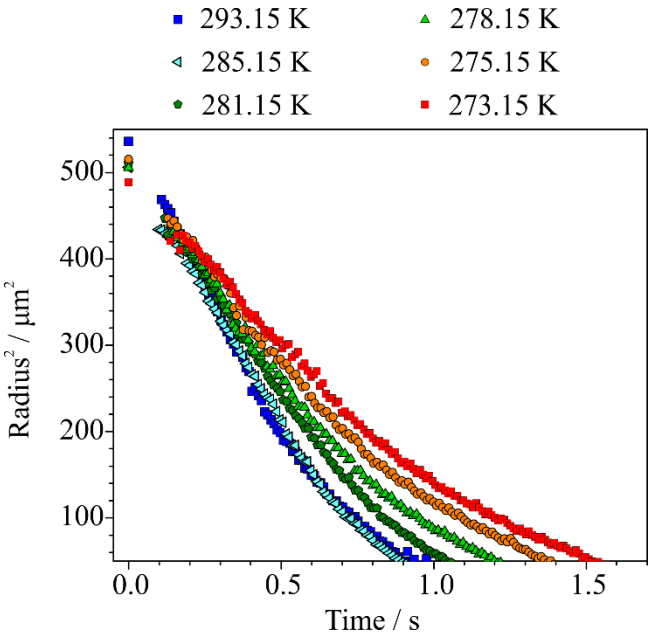

Figure 2: The evaporation profiles of droplets containing 70% ethanol : 30% water (wt/wt) in dry nitrogen over a range of gas phase temperatures.

1

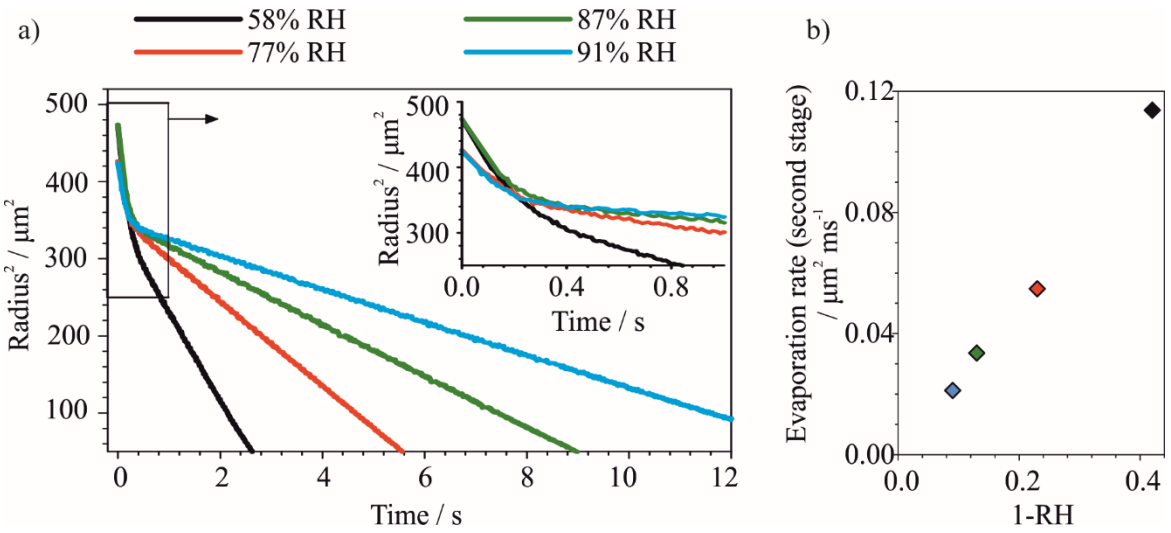

Figure 3: a) The time-dependent radius^2 of droplets containing 50% ethanol : 50% water (wt/wt) as they evaporate into environments of different RH at 293 K. b) The correlation between the evaporation rate of the second regime in the evaporation curve and 1 - the RH.

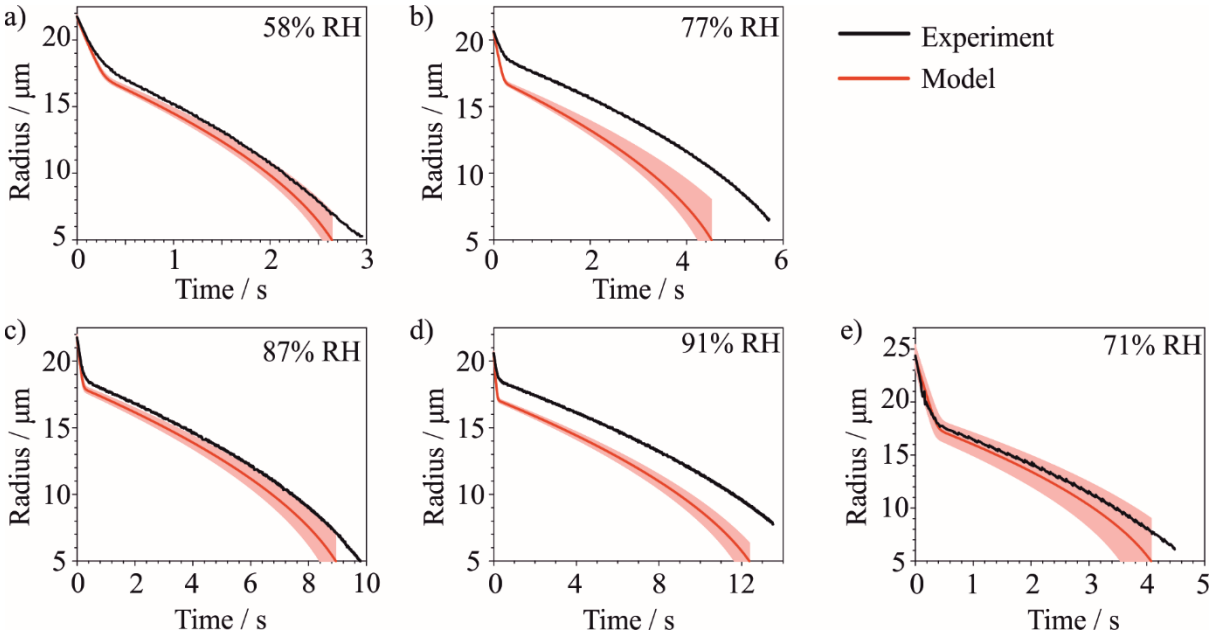

Figure 4: The evaporation of 50% ethanol : 50% water droplets (wt/wt) in the CK-EDB compared to a numerical model at 293 K with a gas phase RH of a) 58%; b) 77%; c) 87% and d) 91 %. e) The evaporation of a 70% ethanol : 30% water droplet (wt/wt) at 293 K at a gas phase RH of 71%. The shading refers to the effect on the model of the uncertainty in the experimental conditions, such as RH, temperature and initial droplet radius.

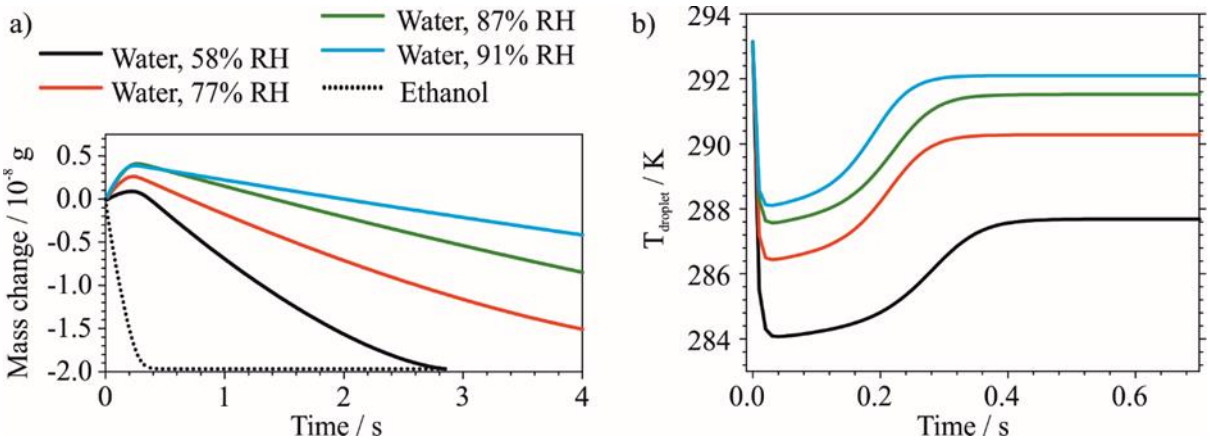

Figure 5: a) Model results of the time-dependent composition of mixed ethanol-water droplets shown in Figure 5 (initial concentration of 50% ethanol : 50% water, wt/wt, respectively). b) Model results of the droplet temperature within the first 0.7 s of evaporation.

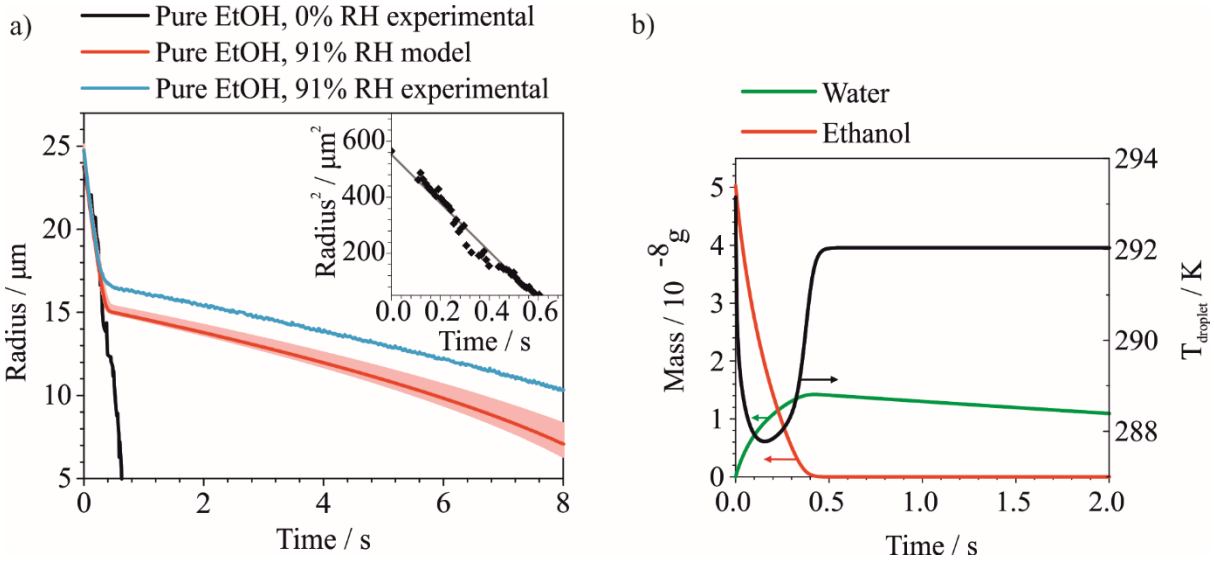

Figure 6: a) The evaporation of a pure ethanol droplet in dry nitrogen compared to within 91% humidity gas phase. The evaporation profile shows that a second evaporation regime occurs when the droplet is surrounded by water vapour, indicating that water condensed onto the droplet within the first 0.4 s of the droplet lifetime. The experimental data is compared to the model results, which predicts a similar evaporation profile. Inset: The radius-squared of the pure ethanol droplet evaporating into dry nitrogen, with a linear fit. b) The temperature of the surface of a pure ethanol droplet as it evaporates into a gas phase RH of 91%. The mass of ethanol in the droplet is also shown, along with the mass of water that condenses onto the droplet and then evaporates after 0.4 s.

1

Notes and references

1 E. I. Mahiques, S. Dederichs, C. Beck, P. Kaufmann and J. B. W. Kok, Coupling multicomponent droplet evaporation and tabulated chemistry combustion models for large-eddy simulations, *Int. J. Heat Mass Transf.*, 2017, **104**, 51–70.

2 A. E. Haddrell, D. Lewis, T. Church, R. Vehring, D. Murnane and J. P. Reid, Pulmonary aerosol delivery and the importance of growth dynamics, *Ther. Deliv.*, 2017, **8**, 1051–1061.

3 A. E. Haddrell, J. F. Davies and J. P. Reid, Dynamics of Particle Size on Inhalation of Environmental Aerosol and Impact on Deposition Fraction, *Environ. Sci. Technol.*, 2015, **49**, 14512−14521.

4 M. Davis and G. Walker, Recent strategies in spray drying for the enhanced bioavailability of poorly water-soluble drugs, *J. Control. Release*, 2018, **269**, 110–127.

5 J. W. Ivey, P. Bhambri, T. K. Church, D. A. Lewis and R. Vehring, Experimental investigations of particle formation from propellant and solvent droplets using a monodisperse spray dryer, *Aerosol Sci. Technol.*, 2018, **52**, 702–716.

6 M. Nuzzo, A. Millqvist-Fureby, J. Sloth and B. Bergenstahl, Surface Composition and Morphology of Particles Dried Individually and by Spray Drying, *Dry. Technol.*, 2015, **33**, 757–767.

7 S. Ingram, C. Cai, Y. Song, D. R. Glowacki, D. O. Topping, S O'Meara and J. P. Reid, Characterising the evaporation kinetics of water and semi-volatile organic compounds from viscous multicomponent organic aerosol particles, *Phys. Chem. Chem. Phys.*, 2017, **19**, 31634–31646.

8 A. M. J. Rickards, Y.-C. Song, R. E. H. Miles, T. C. Preston and J. P. Reid, Variabilities and uncertainties in characterising water transport kinetics in glassy and ultraviscous aerosol, *Phys. Chem. Chem. Phys.*, 2015, **17**, 10059–10073.

9 A. Baldelli, M. A. Boraey, D. S. Nobes and R. Vehring, Analysis of the Particle Formation Process of Structured Microparticles, *Mol. Pharm.*, 2015, **12**, 2562–2573.

10 N. Fu, M. W. Woo and X. D. Chen, Single Droplet Drying Technique to Study Drying Kinetics Measurement and Particle Functionality: A Review, *Dry. Technol.*, 2012, **30**, 1771–1785.

11 A. M. J. Rickards, Y.-C. Song, R. E. H. Miles, T. C. Preston and J. P. Reid, Variabilities and uncertainties in characterising water transport kinetics in glassy and ultraviscous aerosol, *Phys. Chem. Chem. Phys.*, 2015, **17**, 10059–10073.

12 R. E. H. Miles, J. P. Reid and I. Riipinen, Comparison of Approaches for Measuring the Mass Accommodation Coefficient for the Condensation of Water and Sensitivities to Uncertainties in Thermophysical Properties, *J. Phys. Chem. A*, 2012, **116**, 10810–10825.

13 H. Schiffter and G. Lee, Single-Droplet Evaporation Kinetics and Particle Formation in an Acoustic Levitator. Part 1: Evaporation of Water Microdroplets Assessed using Boundary-Layer and Acoustic Levitation Theories, *J. Pharm. Sci.*, 2007, **96**, 2274–2283.

14 M. Kulmala, T. Vesala and P. Wagner, An analytical expression for the rate of binary conensational particle growth, *Proc. R. Soc. Lond. A*, 1993, **441**, 589–605.

15 R. J. Hopkins and J. P. Reid, A comparative study of the mass and heat transfer dynamics of evaporating ethanol/water, methanol/water, and 1-propanol/water aerosol droplets, *J. Phys. Chem. B*, 2006, **110**, 3239–3249.

16 V. Devarakonda and A. K. Ray, Determination of thermodynamic parameters from evaporation of binary microdroplets of volatile constituents, *J. Colloid Interface Sci.*, 2000, **221**, 104–113.

17 C. J. Homer, X. Jiang, T. L. Ward, C. J. Brinker and J. P. Reid, Measurements and simulations of the near-surface composition of evaporating ethanol–water droplets, *Phys. Chem. Chem. Phys.*, 2009, **11**, 7780–7791.

18 S. S. Sazhin, M. Al Qubeissi and J. Xie, Two approaches to modelling the heating of evaporating droplets, *Int. Commun. Heat Mass Transf.*, 2014, **57**, 353–356.

19 J. F. Davies, A. E. Haddrell and J. P. Reid, Time-Resolved Measurements of the Evaporation of Volatile Components from Single Aerosol Droplets, *Aerosol Sci. Technol.*, 2012, 666.

20 G. Rovelli, R. E. H. Miles, J. P. Reid and S. L. Clegg, Accurate Measurements of Aerosol Hygroscopic Growth over a Wide Range in Relative Humidity, *J. Phys. Chem. A*, 2016, **120**, 4376–4388.

21 S. L. Clegg, P. Brimblecombe and A. S. Wexler, Thermodynamic Model of the System H+ - NH4+ - Na+ - SO42- - NO3- - Cl- - H2O at 298.15 K, *J. Phys. Chem. A*, 1998, **102**, 2155–2171.

22 J. R. Rumble, Ed., CRC Press, Taylor & Francis Group, Boca Raton, 98th edn.

23 I. Thormählen, J. Straub and U. Grigull, Refractive Index of Water and Its Dependence on Wavelength, Temperature, and Density, *J. Phys. Chem. Ref. Data*, 1985, **14**, 933–945.

24 N. A. Fuchs, *Evaporation and Droplet Growth in Gaseous Media*, Pergamon Press, Inc., New York, 1959.

25 G. A. Lugg, Diffusion Coefficients of Some Organic and Other Vapors in Air, *Anal. Chem.*, 1968, **40**, 1072–1077.

26 M. J. Tang, M. Shiraiwa, U. Pöschl, R. A. Cox and M. Kalberer, Compilation and evaluation of gas phase diffusion coefficients of reactive trace gases in the atmosphere: Volume 2. Diffusivities of organic compounds, pressure-normalised mean free paths, and average Knudsen numbers for gas uptake calculations, *Atmos. Chem. Phys.*, 2015, **15**, 5585–5598.

27 O. Samimi Abianeh, C. P. Chen and S. Mahalingam, Numerical modeling of multi-component fuel spray evaporation process, *Int. J. Heat Mass Transf.*, 2014, **69**, 44–53.

28 K. P. Mishchenko and V. V Subbotina, Dampfdruck von Ethanol bei Temperaturen von 4 bis 46°C., *Zhurnal Prikl. Khimii*, 1967, **40**, 1156–1159.

29 W. Wagner and A. Pruss, International Equations for the Saturation Properties of Ordinary Water Substance. Revised According to the International Temperature Scale of 1990. Addendum to J. Phys. Chem. Ref. Data 16, 893

(1987), *J. Phys. Chem. Ref. Data*, 1993, **22**, 783–787.

30 A. Zuend, Aerosol Inorganic-Organic Mixtures Functional groups Activity Coefficients, http://www.aiomfac.caltech.edu.

31 A. Zuend, C. Marcolli, B. P. Luo and T. Peter, A thermodynamic model of mixed organic-inorganic aerosols to predict activity coefficients, *Atmos. Chem. Phys.*, 2008, **8**, 4559–4593.

32 Y. Y. Su, R. E. H. Miles, Z. M. Li, J. P. Reid and J. Xu, The evaporation kinetics of pure water droplets at varying drying rates and the use of evaporation rates to infer the gas phase relative humidity, *Phys. Chem. Chem. Phys.*, 2018, **20**, 23453–23466.

33 F. M. Shemirani, S. Hoe, D. Lewis, T. Church, R. Vehring and W. H. Finlay, In Vitro Investigation of the Effect of Ambient Humidity on Regional Delivered Dose with Solution and Suspension MDIs, *J. Aerosol Med. Pulm. Drug Deliv.*, 2012, **26**, 1–8.

34 Y. Kita, Y. Okauchi, Y. Fukatani, D. Orejon, M. Kohno, Y. Takata and K. Sefiane, Quantifying vapor transfer into evaporating ethanol drops in a humid atmosphere, *Phys. Chem. Chem. Phys.*, 2018, **20**, 19430–19440.

35 M. Seaver, A. Galloway and T. J. Manuccia, Water condensation onto an evaporating drop of 1-butanol, *Aerosol Sci. Technol.*, 1990, **12**, 741–744.

36 R. Vehring, W. R. Foss and D. Lechuga-Ballesteros, Particle formation in spray drying, *J. Aerosol Sci.*, 2007, **38**, 728–746.

37 I. S. Khattab, F. Bandarkar, M. A. A. Fakhree and A. Jouyban, Density, viscosity, and surface tension of water+ethanol mixtures from 293 to 323K, *Korean J. Chem. Eng.*, 2012, **29**, 812–817.

38 C. L. Yaws, *Yaws' Handbook of Thermodynamic and Physical Properties of Chemical Compounds*, Knovel, Norwich, 2003.

39 J. M. Coulson, J. F. Richardson, J. R. Backhurst and J. H. Harker, *Coulson & Richardson's Chemical Engineering Vol. 1, Fluid flow, heat transfer and mass transfer*, Butterworth-Heinemann, Oxford, 2009.

40 *DIPPR Project 801 - Full Version*, Design Institute for Physical Property Research/AIChE, 2005.

41 B. Henderson-Sellers, A new formula for latent heat of vaporization of water as a function of temperature, *Q. J. R. Meteorol. Soc.*, 1984, **110**, 1186–1190.

42 J. C. Carstens and J. T. Zung, Theory of droplet growth in clouds. I. The transient stage of the boundary-coupled simultaneous heat and mass transport in cloud formation, *J. Colloid Interface Sci.*, 1970, **33**, 299–311.

43 J. F. Davies, A. E. Haddrell, A. M. J. Rickards and J. P. Reid, Simultaneous analysis of the equilibrium hygroscopicity and water transport kinetics of liquid aerosol, *Anal. Chem.*, 2013, **85**, 5819–5826.

44 A. Marsh, R. E. H. Miles, G. Rovelli, A. G. Cowling, L. Nandy, C. S. Dutcher and J. P. Reid, Influence of organic compound functionality on aerosol hygroscopicity: Dicarboxylic acids, alkyl-substituents, sugars and amino acids, *Atmos. Chem. Phys.*, 2017, **17**, 5583–5599.

45 J. W. Ivey, P. Bhambri, T. K. Church, D. A. Lewis, M. T. McDermott, S. Elbayomy, W. H. Finlay and R. Vehring, Humidity affects the morphology of particles emitted from beclomethasone dipropionate pressurized metered dose inhalers, *Int. J. Pharm.*, 2017, **520**, 207–215.

46 B. Asgharian, A model of deposition of hygroscopic particles in the human lung, *Aerosol Sci. Technol.*, 2004, **38**, 938–947.